Hydrodynamic orienting of asymmetric microobjects under gravity

Maria L Ekiel-Jeżewska and Eligiusz Wajnryb

Institute of Fundamental Technological Research, Polish Academy of Sciences,
Świętokrzyska 21, 00-049 Warsaw, Poland

E-mail: mekiel@ippt.gov.pl

Abstract
It is shown that non-symmetric microobjects orient while settling under gravity in a viscous
fluid. To analyze this process, a simple shape is chosen: a non-deformable 'chain'. The chain
consists of two straight arms, made of touching solid spheres. In the absence of external
torques, the spheres are free to spin along the arms. The motion of the chain is evaluated by
solving the Stokes equations with the use of the multipole method. It is demonstrated that the
spinning beads speed up sedimentation by a small amount and increase the orientation rate
significantly in comparison to the corresponding rigid chain. It is shown that chains orient
towards the V-shaped stable stationary configuration. In contrast, rods and star-shaped
microobjects do not rotate. The hydrodynamic orienting is relevant for efficient swimming of
non-symmetric microobjects and for sedimenting suspensions.

1. Introduction

In many biological, medical and industrial applications, it is
of interest to predict theoretically what is the sedimentation
velocity of small conglomerates of micro-particles under
gravity in a fluid [1–5] and how the settling speed can be
enhanced or decreased, by a suitable modification of the
configuration, or directly by a change of the relative motion of
the particles. This issue is especially important for mechanisms
of effective swimming, recently intensively investigated for
biological systems as well as for artificial micro and nano-
swimmers.

Swimming patterns of various microorganisms have
been extensively investigated experimentally and theoreti-
cally [6–17]. Microorganisms propel themselves owing to a
periodic change of their shape and possibly also its orientation
in space. Often the core cell does not deform, and the shape
is changed owing to waving, undulating or rotating flagella.
Typical sizes of bacteria, spermatozoa or algae lie in the range
from 1 to 200 μm, and their swimming speeds are usually up
to several hundred μm s^{-1}. For such microobjects moving
in aqueous environments, the fluid inertia and the Brownian
motion are irrelevant [11]. Therefore, a theoretical model of
swimming should be based on hydrodynamic interactions [18]
between individual parts of the microobject, following from
the stationary Stokes equations and the appropriate boundary

conditions at the surface of the swimmer. Typically, in the
swimming problem a periodic sequence of flagella shapes
and the corresponding translational and rotational velocities of
their parts relative to the core cell are known as functions of
time, as well as the total force and torque exerted on the cell
center. The task is to determine the translational velocity of
the center, and also the cell's angular velocity. There exist a
number of models of freely moving swimmers (the total force
and torque vanish).

However, the microorganisms are often denser than
the water in which they swim, by a few per cent
for the algae, approximately 10% for bacteria and 30%
for spermatozoa, and the mass distribution can be non-
uniform [11]. The gravitational force is essential for
explanation of the orientational mechanisms (gravitaxis)
observed experimentally, e.g. for algae [19, 20]. In general,
hydrodynamic interactions would tend to orient non-symmetric
microobjects settling under gravity. This effect, certainly
important for swimming, will be investigated in this paper.

We focus on a very simple model: a non-symmetric
'chain' of three identical spheres, with two pairs at contact, but
not the third one. Owing to the lubrication forces, the shape of
the conglomerate is fixed. In section 2, the accurate spherical
multipole method [21, 22] of solving the Stokes equations
is introduced, with the lubrication correction for the relative
motion of close surfaces [23], and the HYDROMULTIPOLE

numerical code [23]. In section 3, we use this method to
evaluate the translational, rotational and spinning velocities
of the microobject, determine how it orients while settling
under gravity, and find the stable stationary configuration. In
section 4, we study how the settling speed depends on shape,
by comparing sedimentation velocities of all the stationary
configurations of three spheres [24–26]. We also investigate
how accurate is the point-particle approximation [27]. In
section 5 we summarize the results obtained for the chain
made of three spheres. We also check if chains with two arms
made of a larger number of beads orient hydrodynamically,
qualitatively in the same way as the simple three-sphere model.

2. The model of a moving asymmetric microobject

Consider three identical spheres falling under gravitational
forces $\tilde{\boldsymbol{F}}_0$ in an infinite fluid of viscosity η. A low Reynolds
number is assumed for the corresponding fluid flow. The fluid
velocity $\mathbf{v}(r)$ and pressure $p(r)$ satisfy the stationary Stokes
equations [18, 28],

$$\eta\nabla^2\mathbf{v} - \nabla p = \mathbf{0}, \qquad \nabla\cdot\mathbf{v} = 0, \qquad (1)$$

with the stick boundary conditions at the surfaces of the
spheres and no fluid flow at infinity. Therefore the translational
$\tilde{U}_i$ and rotational $\tilde{\Omega}_i$ velocities of each sphere $i = 1, 2, 3$ are
linear functions of the force $\tilde{\boldsymbol{F}}_0$,

$$\tilde{U}_i = \left[\sum_{k=1}^{3}\tilde{\boldsymbol{\mu}}_{ik}^{tt}\right]\cdot\tilde{\boldsymbol{F}}_0, \qquad (2)$$

$$\tilde{\Omega}_i = \left[\sum_{k=1}^{3}\tilde{\boldsymbol{\mu}}_{ik}^{rt}\right]\cdot\tilde{\boldsymbol{F}}_0, \qquad i = 1, 2, 3. \qquad (3)$$

The 3×3 mobility matrices $\tilde{\boldsymbol{\mu}}_{ik}^{tt}$ and $\tilde{\boldsymbol{\mu}}_{ik}^{rt}$ are to be found as
functions of the relative positions $\tilde{r}_l - \tilde{r}_j$ of the sphere centers.

In the following, as in [25], particle positions $\tilde{r}_i$ will be
normalized by the sphere diameter d, translational velocities
$\tilde{U}_i$ by the Stokes velocity, $U_S = |\tilde{\boldsymbol{F}}_0|/(3\pi\eta d)$, angular
velocities $\tilde{\Omega}_i$ by $2U_S/d$, and time $\tilde{t}$ by two Stokes times,
$2\tau_S = d/U_S$. The corresponding dimensionless quantities
are $r_i = \tilde{r}_i/d$, $U_i = \tilde{U}_i/U_S$, $t = \tilde{t}/(2\tau_S)$, $\Omega_i = \tilde{\Omega}_i\tau_S$,
$\boldsymbol{\mu}_{ik}^{tt} = \tilde{\boldsymbol{\mu}}_{ik}^{tt}\cdot 3\pi\eta d$, $\boldsymbol{\mu}_{ik}^{rt} = \tilde{\boldsymbol{\mu}}_{ik}^{rt}\cdot 3\pi\eta d^2/2$, $\boldsymbol{F}_0 = \tilde{\boldsymbol{F}}_0/|\tilde{\boldsymbol{F}}_0|$.

In our model it is assumed that each sphere touches
another one. Once this happens, the spheres remain in
contact owing to lubrication forces [29]. Such configurations
will be called 'chains'. As illustrated in figure 1, posi-
tions of the sphere centers, $r_1 = (-x/2, 0, z)$, $r_2 = (0, 0, 0)$,
$r_3 = (x/2, 0, z)$, are parametrized by the angle α
between the chain links, with $x = 2\sin(\alpha/2)$ and
$z = \cos(\alpha/2)$. Orientation of the gravitational force is
arbitrary, $\boldsymbol{F}_0 = (F_{0x}, F_{0y}, F_{0z})$.

Evaluation of the mobility matrices of chains requires a
special treatment, because now there are at least two contact
points. Moreover, it is essential to specify more precisely what
is meant by 'the contact'. The first possibility is to assume that
there is no external forces other than gravity exerted on each
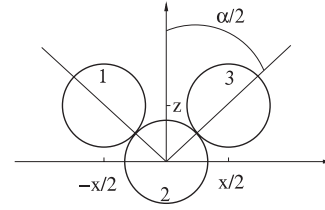of the spheres. In this case, lubrication does not allow for any

Figure 1. Parametrization of a chain configuration.

relative motion of the touching spheres except their spinning
along the line of centers [29]. In the following, such a contact
will be called 'beads'. The second option is to 'glue' the
touching spheres, imposing on them external torques, which
prevent them from any relative motion. Such a contact will be
called 'rigid'. In appendix A, it is explained in detail what the
difference is between the mobility matrices for both types of
chains.

The essential task of this paper is to determine the 3×3
mobility matrices $\boldsymbol{\mu}_{ik}^{tt}$ and $\boldsymbol{\mu}_{ik}^{rt}$ both for chains made of beads
and the rigid ones. Because of hydrodynamic interactions of
the close surfaces, we have to go beyond the point-particle
approximation, and even beyond superposition of two-body
mobilities [18, 21].

Therefore we evaluate the three-sphere mobilities numeri-
ically by the multipole expansion [18, 21]. The algorithm
from [22] and its accurate numerical FORTRAN implemen-
tation HYDROMULTIPOLE [23] are applied. The accuracy
is controlled by a varied order of the multipole truncation L
(see [22] for the definition of L and [22, 30] for a discussion
of the accuracy estimates). In this paper, we take a large value
$L = 6$. The results will be presented in section 3.

3. Motion of a chain

It is convenient to describe the motion of a chain (rigid or made
of beads) referring to its center of mass, $\mathbf{R} = (r_1 + r_2 + r_3)/3$,
because in this case the total external torque vanishes. The task
is to find its translational velocity, $\boldsymbol{U} = (U_1 + U_2 + U_3)/3$,
and the rotational one, $\boldsymbol{\Omega} = \Omega_2 = (\Omega_1 + \Omega_2 + \Omega_3)/3$.
For the chain made of beads, the spinning speed ω^{beads}
along the chain arms also needs to be determined; from the
symmetry of the system it follows that $\omega^{\text{beads}}\hat{r}_{12} = \Omega_1 - \Omega_2$,
and $-\omega^{\text{beads}}\hat{r}_{32} = \Omega_3 - \Omega_2$, with the unit vector
$\hat{r}_{ij} = r_{ij}/|r_{ij}|$, and the standard notation for the relative
positions, $r_{ij} = r_i - r_j$.

The translational and angular velocities of the chain
depend linearly on the total gravitational force acting on the
chain, $\boldsymbol{F} = 3\boldsymbol{F}_0$,

$$\boldsymbol{U} = \boldsymbol{\mu}^{tt}\cdot\boldsymbol{F}, \qquad (4)$$

$$\boldsymbol{\Omega} = \boldsymbol{\mu}^{rt}\cdot\boldsymbol{F}, \qquad (5)$$

$$\omega = \boldsymbol{\mu}^{\omega}\cdot\boldsymbol{F}, \qquad (6)$$

with the mobility matrices of the chain to be found. Owing to
the symmetry, in the frame of reference shown in figure 1,

$$\boldsymbol{\mu}^{tt} = \frac{1}{3}\begin{pmatrix} \mu_1(\alpha) & 0 & 0 \\ 0 & \mu_2(\alpha) & 0 \\ 0 & 0 & \mu_3(\alpha) \end{pmatrix}, \qquad (7)$$
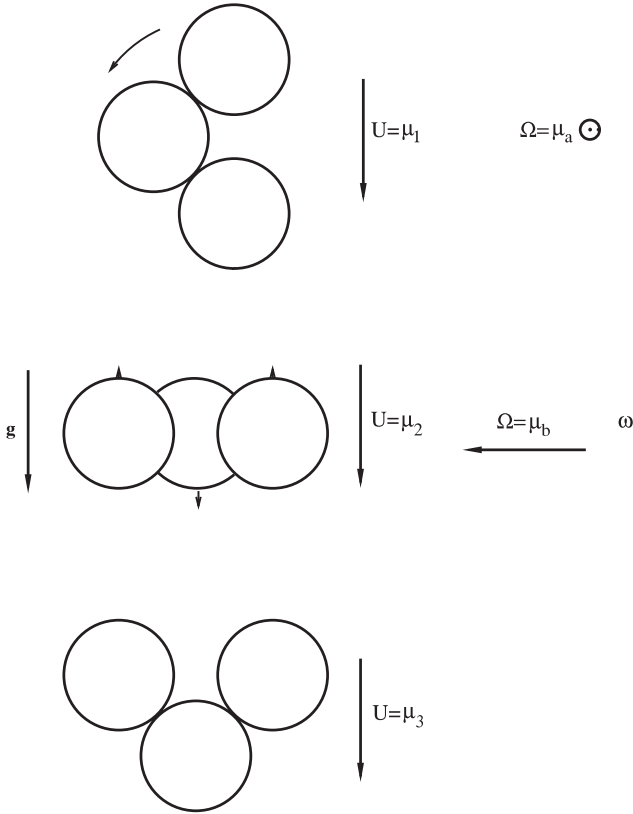
Figure 2. Degrees of freedom of chains at the characteristic orientations with respect to gravity. Top: gravity along x; middle: gravity along y; down: gravity along z.

$$\boldsymbol{\mu}^{rt} = \frac{1}{3} \begin{pmatrix} 0 & \mu_b(\alpha) & 0 \\ -\mu_a(\alpha) & 0 & 0 \\ 0 & 0 & 0 \end{pmatrix}, \qquad (8)$$

$$\boldsymbol{\mu}^{\omega} = \frac{1}{3} \begin{pmatrix} 0 & \mu_\omega(\alpha) & 0 \end{pmatrix}. \qquad (9)$$

In the above equations, the factor 1/3 has been introduced. With this choice, in the frame of reference shown in figure 1, and with the adopted normalization, the mobility coefficients for the chain are just equal to the corresponding velocity components, $\mu_1 = U_x$, $\mu_2 = U_y$, $\mu_3 = U_z$, $\mu_a = -\Omega_y$ and $\mu_b = \Omega_x$. The physical meaning of the coefficients is indicated in figure 2.

The mobility coefficients in equations (7) and (8) are determined from combinations of the three-sphere friction coefficients for the individual spheres, as outlined in appendix A. In general, the mobility coefficients for a chain of beads differ from those for a rigid chain at the same configuration and in this case they will be denoted by the corresponding superscripts. Thus, $\mu_2^{\text{beads}} \neq \mu_2^{\text{rigid}}$ and $\mu_b^{\text{beads}} \neq \mu_b^{\text{rigid}}$. For a rigid chain, there is no spinning and $\mu_\omega^{\text{rigid}} = \omega^{\text{rigid}} = 0$, while the chain of beads does spin, $\mu_\omega^{\text{beads}} = \omega^{\text{beads}} \neq 0$. However, for a rigid chain and the chain of beads at the same configuration, μ_1, μ_3 and μ_a are identical and those coefficients will not be marked by any superscripts.

The translational motion will now be determined. The corresponding mobility coefficients are evaluated numerically and plotted in figure 3 as functions of the angle α. For
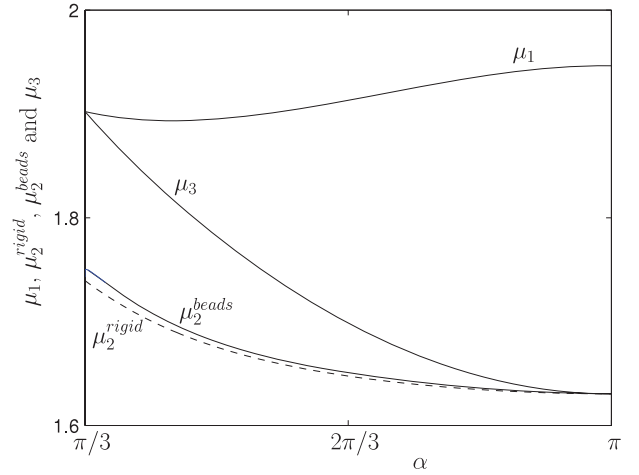

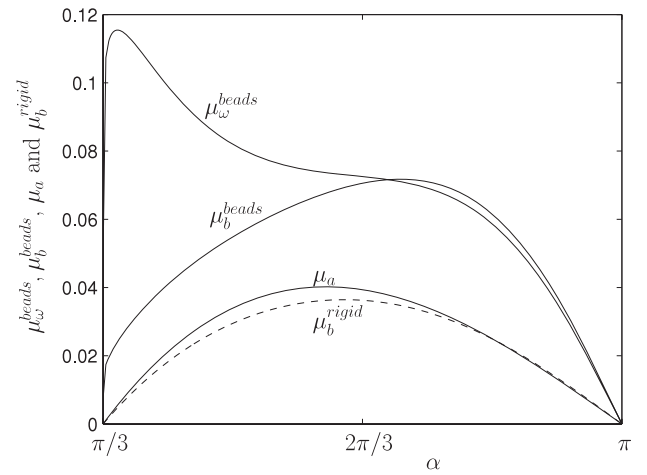**Figure 3.** The chain translational velocity components.

Figure 4. The chain angular and spinning velocity components.

$\alpha = \pi/3$, the sphere centers form an equilateral triangle with three contact points; in the following, this configuration will be called 'a star'. For $\alpha = \pi$, the sphere centers are aligned; this configuration will be called 'a rod'. For μ_2 and μ_3, when the base of the chain is perpendicular to gravity, then its settling velocity is a decreasing function of the apex angle α, in agreement with the intuitive prediction that stretching the arms should increase the friction force. For μ_1, when the base of the chain is parallel to gravity, it is intuitive to expect the opposite effect: with the increase of α, the chain aligns along gravity, and its resistance is weaker. This is indeed observed for a wide range of the larger angles, except those relatively close to $\pi/3$.

For a given shape (fixed α), we now compare the magnitude of μ_1, μ_2 and μ_3. Settling is always fastest if gravity is along the base of the chain, and slowest if gravity is perpendicular to the plane of the chain. Notice that in the last case, the chain made of spinning beads sediments faster than the corresponding rigid one.

The spinning speed and rotational velocities are plotted in figure 4. The spinning speed reaches a maximum for a very small value of α, and then slowly decreases. For a
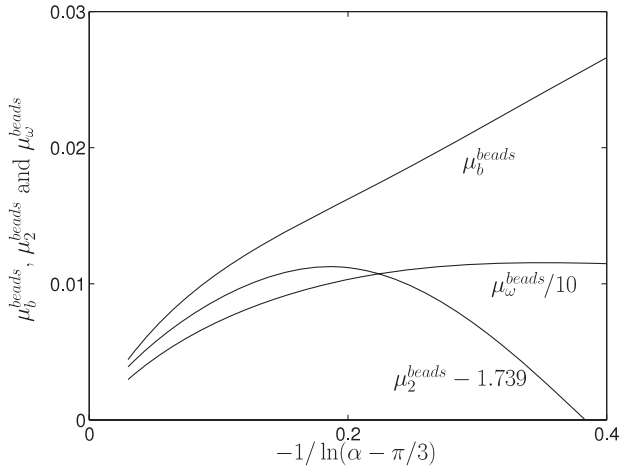
Figure 5. The mobility coefficients for a spinning chain of beads with a small α.

wide range of the angles between the chain arms, the spinning surfaces move with velocities which are still around 5% of the settling speed. Next, we evaluate the chain rotation. The corresponding mobility coefficients are plotted in figure 4 as functions of α. Each component of the angular velocity is zero for stars and rods, and has a maximum at intermediate values of the angle between the arms, smaller than $2\pi/3$ for a rigid chain. Therefore the speed of the hydrodynamic orienting is very sensitive to shape. It is remarkable that spinning of the beads has a profound effect on the chain rotation. The spinning increases the angular velocity by at least a factor of two in comparison to the corresponding rigid chain at the same configuration. Moreover, we observe a much wider range of chain shapes for which the rotation is significant. Indeed, the maximum is shifted to larger values of α, above $2\pi/3$, and there is a qualitative difference at small angles, where the lubrication interactions between the spinning beads keep the chain rotating.

When the close surfaces of spheres 1 and 3 move with respect to each other, then the mobility coefficients μ_2^{beads}, μ_b^{beads} and $\mu_\omega^{\text{beads}}$ decrease rapidly with decreasing α only if $\alpha - \pi/3$ becomes extremely small, as seen in figures 3 and 4. This is the typical lubrication interaction of very close surfaces in relative motion [29]. Actually, the relative mobility coefficients decrease to zero as the inverse logarithm of the gap size. This scaling can be seen in figure 5, where μ_2^{beads}, μ_b^{beads} and $\mu_\omega^{\text{beads}}$ are plotted as functions of $[-1/\ln(\alpha - \pi/3)]$. In fact, to account for the relative motion, we plot $\mu_2(\alpha) - \mu_2(\pi/3)$ rather than $\mu_2(\alpha)$, with the zero-gap mobility $\mu_2(\pi/3) = 1.739$ (see section 4.1 for the derivation). Numerical results are not available when the size of the gap between two surfaces is comparable with the numerical accuracy. For smaller values of α, asymptotic expressions analogous to equations (12) and (13) in [25] could be derived using the same procedure. Notice that in the lubrication regime, the spinning speed of the beads is significantly larger than the angular velocity of the chain.

It remains to discuss the main issue of this paper, that is how the chains orient with time. Taking the laboratory frame of

reference (X, Y, Z), in which $\boldsymbol{F}_0 = (0, 0, -1)$, we parametrize the chain configuration by the Euler angles θ, ψ and φ. Here θ is the angle between the Z axis and the chain symmetry axis z, with $\cos\theta = -\boldsymbol{F}_0 \cdot \hat{\boldsymbol{z}}$, and ψ is the angle between the line of nodes and the axis x, and ϕ is the angle between the axis X and the line of nodes. From equations (5) and (8) we obtain,

$$\dot{\theta} = -(\mu_a \sin^2\psi + \mu_b \cos^2\psi)\sin\theta, \qquad (10)$$

$$\dot{\psi} = -(\mu_a - \mu_b)\cos\psi\sin\psi\cos\theta, \qquad (11)$$

$$\dot{\varphi} = (\mu_a - \mu_b)\cos\psi\sin\psi, \qquad (12)$$

If $\psi \neq n\pi/2$ where $n = 0, 1, 2, \ldots$, and $\lambda = \mu_a/(\mu_a - \mu_b)$ then the solution is

$$\sin^2\theta = C\tan^{2\lambda}\psi/\sin^2\psi. \qquad (13)$$

For $\pi/3 < \alpha < \pi$, the calculated mobility coefficients μ_a and μ_b are positive, and therefore from equation (10) it immediately follows that θ evolves towards zero, e.g. towards the chain axis antiparallel to gravity. This orientation of the chain will be called 'V-shaped'. It is the only stable orientation of the chain with $\pi/3 < \alpha < \pi$.

Two examples of a one-dimensional dynamics are recovered from equation (10) for two symmetric cases with $\psi = 0$ and $\psi = \pi/2$, respectively. For $\psi = 0$, equation (10) reads,
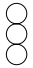
$$\dot{\theta} = -\mu\sin\theta, \qquad (14)$$
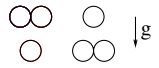
with $\mu = \mu_a$ and the solution,

$$\tan(\theta/2) = A\exp(-\mu t). \qquad (15)$$

This dynamics is illustrated in figure 2, with its upper C-shaped configuration, which corresponds to $\theta(t = 0) = \pi/2$, evolving towards the bottom one (V-shaped). The sense of the rotation is illustrated by the arrow. For $\psi = \pi/2$, equation (14) also holds, but now with $\mu = \mu_b$. This dynamics is also illustrated in figure 2, now with its middle plane configuration, which corresponds to $\theta(t = 0) = \pi/2$, evolving towards the bottom one (V-shaped). The sense of the rotation is illustrated by arrows of different lengths.

To complete the analysis, we still need to compare a typical timescale of the hydrodynamic orienting to that characteristic for the settling motion. We therefore find the angles $\alpha_{a,\text{max}}$ and $\alpha_{b,\text{max}}$ which correspond to the maxima of μ_a and μ_b, respectively, and then calculate the ratio of both time scales, $2\pi\mu_1/\mu_a$ and $2\pi\mu_2/\mu_b$, at $\alpha_{a,\text{max}}$ and $\alpha_{b,\text{max}}$, respectively. For the rigid chain, both ratios are of the order of 300. For the spinning beads, $2\pi\mu_2/\mu_b$ and $2\pi\mu_2/\mu_\omega$ at α_{max} are of the order of 150. Therefore the characteristic timescale of the hydrodynamic orienting is at least two orders of magnitude larger than that of the gravitational settling. Reorientation of the sedimenting non-symmetric particles is significant for such systems which stay under gravity for a sufficiently long time.

Table 1. Settling velocities U of stationary configurations of three spheres.

	Rod ∥ F	Rod ⊥ F	Vertical chain	Star ∥ F	Star ⊥ F	Kissing	Ring
Spheres	1.95	1.63	1.63–1.90	1.90	1.74	1.75	1.74–1.79–1
Point-particle approximation	2.00	1.61	1.61–2.04	2.04	1.75	1.81	1.75–1.74–1

4. Stationary configurations

The goal of this section is to show which chain configurations do not orient under gravity. Settling speeds of such stationary configurations will in addition be compared to the translation velocities of other stationary configurations of three spheres, with the emphasis on those with the spinning particles.

By definition, at a stationary configuration the spheres have equal translational velocities, $U_i = U$. Such a configuration is an equilibrium solution of the dynamics of the relative positions. Notice that U is time-independent. In our case, obviously, $i = 1, 2, 3$.

4.1. Stationary chains

For chains, the equilibrium condition $U_i = U$ is equivalent to the relation, $\Omega = 0$, which takes the form

$$\mu_a(\alpha)F_x = \mu_b(\alpha)F_y = 0, \tag{16}$$

if equations (5) and (8) are applied. According to the numerical results plotted in figure 4, equation (16) has the solutions,

 (i) an arbitrary α, and $F_x = F_y = 0$,
 (ii) an arbitrary F, and $\alpha = \pi/3$, or π.

Condition (i) corresponds to the vertical chain equilibria, found in [25] and sketched in table 1. These are the chains with the symmetry axis parallel to gravity. Condition (ii) corresponds to stars and rods, also sketched in table 1.

Notice that from the symmetry it follows that the beads of the stationary chains do not spin, $\omega = 0$. The settling velocities U of the stationary chains will now be evaluated. The results will also be compared with the point-particle model. For touching spheres, such an approximation has to take into account additional constraint forces, which do not allow the points that approximate the touching spheres to change the interparticle distance [27].

Consider first the vertical chains. From symmetry with respect to reflections $x, X \rightarrow -x, -X$ and $y \rightarrow -y$ it follows that U is vertical. Values of the settling velocities, $U(\alpha) = \mu_3(\alpha)$, evaluated in [25], and replotted here in figure 3, span the range $\mu_3(\pi) \leqslant U \leqslant \mu_3(\pi/3)$, with

$$\mu_3(\pi) = 1.630\,458\,19, \tag{17}$$

$$\mu_3(\pi/3) = 1.902\,2670. \tag{18}$$

Similar values follow from the point-particle approximation with constraints, $29/18 \leqslant U^{\text{points}} \leqslant 229/112$.

The settling velocities $U_\parallel$ and $U_\perp$ of the rods parallel and perpendicular to gravity are now evaluated for the subsequent values of the multipole order $L \leqslant 30$, and extrapolated to $L \rightarrow \infty$. Then,

$$U_\parallel = \mu_1(\pi) = 1.946\,299\,144, \tag{19}$$

$$U_\perp = \mu_2(\pi) = 1.630\,458\,19. \tag{20}$$

These values are again well approximated by the point-particle approximation with constraints, with $U_\parallel^{\text{points}} = 2$ and $U_\perp^{\text{points}} = 29/18$. Both parallel and perpendicular rods settle down vertically, i.e. along gravity. The calculated velocities (19) and (20) agree with the previous experimental and numerical results [1, 3].

In a similar way we calculate velocities of the stars. Notice that owing to the symmetry with respect to rotation by $\pi/3$, the stars located in the vertical plane settle with the same velocity, independently of their orientation. However, their settling velocity $U_\parallel$ is larger than that of the stars oriented horizontally, $U_\perp$. In both cases, the stars translate vertically. We evaluate,

$$U_\parallel = \mu_1(\pi/3) = 1.902\,267\,03, \tag{21}$$

$$U_\perp = \mu_2(\pi/3) = 1.739\,412\,60. \tag{22}$$

In the point-particle approximation with constraints, $U_\parallel^{\text{points}} = 229/112$ and $U_\perp^{\text{points}} = 7/4$. The results (21) and (22) obtained for the stars improve the accuracy of the previous simulations [5], and agree well with the measurements [2].

In general, the stars and rods are inclined at a certain angle with respect to gravity. In this case, their velocities are not vertical, and the components follow from equation (7). A special case of such inclined stars was discussed in [25], where it was indicated by the dotted line in figure 15. In this 'slanted equilateral chain' configuration, a line of centers was perpendicular to gravity.

Using the dynamics derived in section 3, we conclude that the only stable stationary solutions of the dynamics of chains are the V-shaped vertical chains. The hat-shaped vertical chains are unstable. Rods and stars are neutrally stable if the three contact points are kept. The stars and rods are generally unstable against perturbations which separate out a pair of touching spheres.

4.2. Comparison with other stationary configurations

The settling speeds of stationary chains will be now compared with the motion of other equilibrium configurations of three spheres. At equilibrium, the triangle formed by the sphere centers has the following shape, size and orientation with respect to gravity.
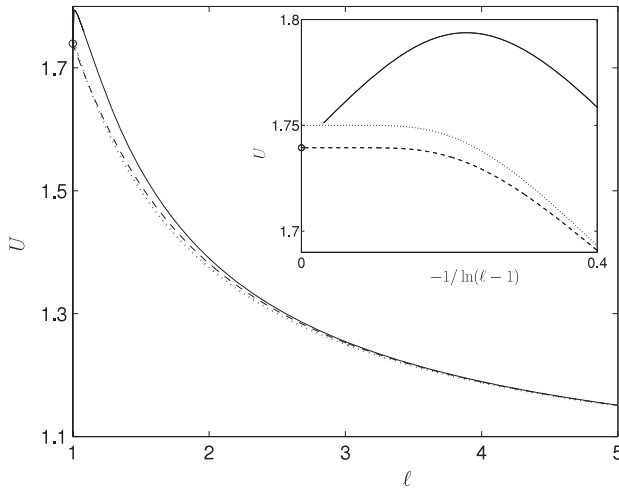
Figure 6. Settling velocity U of the ring (equilateral horizontal triangle) versus its side length ℓ. Equilibrium (solid line); rigid system with constraints (dashed line), point-particle approximation (point line) and the horizontal star ($\circ$). Inset: U as a function of $[-1/\ln(\ell - 1)]$ for very close particles.

- 'Vertical chain' (a vertical isosceles triangle with the symmetry axis along gravity; the apex sphere touches each of the base spheres).
- 'Rod' (a straight line of an arbitrary orientation with respect to gravity; there are two contact points between the sphere surfaces).
- 'Star' (an equilateral triangle at an arbitrary orientation with respect to gravity; there are three contact points between the sphere surfaces).
- 'Kissing' (an isosceles triangle with the symmetry axis along gravity and touching base particles; the distance between the contact point and the center of the apex particle equals 1.578 634 diameter, see [25] and[1]).
- 'Ring' (an equilateral triangle of an arbitrary side length, in the plane perpendicular to gravity, see [26, 31]).

In table 1, the stationary configurations are sketched and values of their vertical velocities are listed, together with their approximation by point-particles with constraints. We have demonstrated that for a small number of particles, the settling velocities of their stationary configurations can be within a few per cent approximated by the point-particle model with constraints. Notice that all the equilibria except the ring are unstable, if arbitrary perturbations are allowed, including separation of the touching surfaces [25].

The ring is the only equilibrium configuration with rotation of the individual spheres. It is therefore interesting to investigate whether the spinning increases the settling velocity, as has been observed for chains made of beads. This problem will be discussed in detail in section 4.3.

4.3. Stationary configurations with spinning

We now focus on the stationary configurations called rings. The sphere centers form a horizontal equilateral triangle with

---

[1] Settling velocity of the kissing equilibria, $U = 1.754\,3000$, was evaluated in [25]. Here we check that it is reasonably well approximated by $U^{\text{points}} = 1.814\,803$.
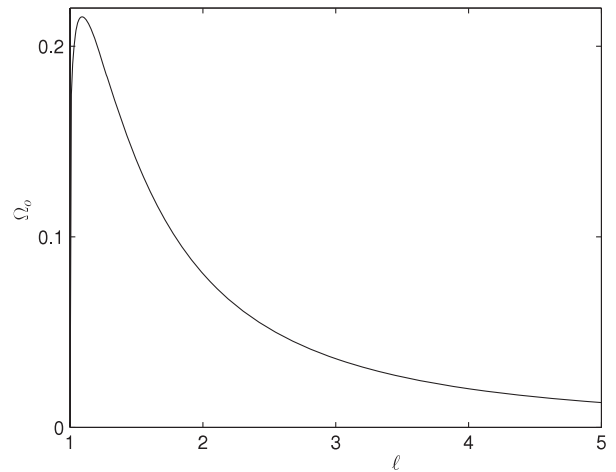

Figure 7. Spinning velocity Ω_o versus the size ℓ of the ring.

an arbitrary length $\ell \geqslant 1$ of its side. Settling velocity $\boldsymbol{U}$ is of course vertical. Its value $U = |\boldsymbol{U}|$ is evaluated and plotted in figure 6 as a function of ℓ. In general, the particles are separated from each other; they touch only in the limiting case of $\ell = 1$, when the ring becomes the horizontal star, with $U = 1.739\,412\,60$.

It is interesting to observe that if the particles are free to spin, then the ring's settling velocity has a maximum for a very small gap between the sphere surfaces. The maximum is clearly visible in the inset of figure 6. Bracketing this maximum by the standard golden section search [32], we evaluate the corresponding values of ℓ_{MU} and $U(\ell_{MU})$. The subsequent multipole orders $1 \leqslant L \leqslant 28$ are used, and the results are next extrapolated to $L \rightarrow \infty$, as in [25]. We obtain, $\ell_{MU} = 1.011\,28$ and $U(\ell_{MU}) = 1.793\,94$. For larger values of ℓ, the settling velocity decreases to one (the Stokes value) with $\ell \rightarrow \infty$. In table 1, the ring velocities at $\ell = 0$, ℓ_{MU} and ∞ have been indicated.

To check whether the existence of the maximum is related to the spinning, we also consider a rigid system of three spheres at the same configurations, but with the spinning eliminated owing to constrained external torques. Velocities of such configurations are also plotted in figure 6. They are systematically smaller than the velocities of the ring. Indeed, this example also indicates that spinning speeds up the rate of settling by a small amount.

The point-particle approximation, $U = 1 + 3/(4\ell)$, is also depicted in figure 6. Notice that for rings, no constraint forces nor torques are applied, since the rings are also stationary solutions of the point-particle dynamics. It is clear that the point-particle approximation is much closer to the rigid dynamics than to the spinning system.

Finally, we evaluate the spinning velocities of the spheres. Here $\boldsymbol{\Omega}_1 = \Omega_o \hat{\boldsymbol{r}}_{32}$, $\boldsymbol{\Omega}_2 = \Omega_o \hat{\boldsymbol{r}}_{13}$, and $\boldsymbol{\Omega}_3 = \Omega_o \hat{\boldsymbol{r}}_{21}$, with Ω_o, plotted in figure 7 as a function of the side length ℓ. The maximum of Ω_o is reached at the small distance between the sphere centers, $\ell_{M\Omega} = 1.092\,3791$, but not as small as ℓ_{MU}. At the maximum, the spinning velocity $\Omega_o(\ell_{M\Omega}) = 0.215\,537\,174$, is as much as 12% of the settling speed, $U(\ell_{M\Omega}) = 1.751\,9797$. At the maximum of U, the

spinning is slightly smaller, with $\Omega_o(\ell_{MU}) = 0.177\,04$. These two maxima are shifted with respect to each other, because U becomes larger not only by an increase of Ω_o, but also by a decrease of the distance between the spheres.

Notice that for the ring configuration of the separated spheres, the maximal spinning velocity is twice as large as that for the horizontal chain of the touching beads. As a consequence, the increase of the settling velocity is also twice as large.

5. Conclusions

The goal of this paper has been to construct and study a simple model of a chain-like asymmetric microobject of a fixed shape, settling under gravity in a viscous fluid. The motion of such a system has been evaluated from the multipole expansion of the Stokes equations. The main results are the following.

It has been found that asymmetric microobjects orient hydrodynamically while settling under gravity. This effect is not observed for axially symmetric objects such as rods, nor for regular shapes such as equilateral triangles, here called stars. However, chain-like conglomerates made of two identical straight arms in general orient towards a vertical 'head down' equilibrium configuration; that is, towards a V-shape. This process is relatively slow in comparison to the cluster sedimentation, but definitely not negligible. We have checked that the hydrodynamic orienting is observed for chains made of a central particle with the attached two identical straight arms made of a certain number of spinning or rigid beads, for example ten spheres at each arm. The central particle may be the same size as the other ones, or larger, e.g. 10 times larger, and even slightly less dense than the arm beads.

It has been shown that freely rotating particles in chain-like conglomerates can spin even if their surfaces touch each other. The spinning can be even faster than the chain rotation. The spinning particles speed up the conglomerate settling by a few per cent, and they significantly enhance its tendency to orient vertically, in comparison to the rigid body. Spinning also speeds up the settling of stationary configurations of spheres separated from each other.

Naturally, the hydrodynamic orienting found in this work is important for efficient swimming of microorganisms which are more dense than the fluid. The results are also relevant for suspensions of chain-like conglomerates settling under gravity. On a long timescale, while reorienting takes place, the suspension structure and settling speed may change, leading to ordering of the sediment and possible applications to segregation and filtration techniques.

Acknowledgment

Appendix A. How to evaluate mobility of a conglomerate

For a system of N particles separated from each other, the 6×6 mobility matrices $\boldsymbol{\mu}_{ij}$ form a $6N \times 6N$ tensor, which is evaluated as the inverse of the $6N \times 6N$ friction tensor, made of 6×6 friction matrices $\boldsymbol{\zeta}_{ij}$. The latter relate the external forces and torques, $\boldsymbol{F}_i$ and $\boldsymbol{T}_i$, exerted on a particle $i = 1, \ldots, N$, to the translational and angular velocities, $\boldsymbol{U}_j$ and $\boldsymbol{\Omega}_j$, of a particle $j = 1, \ldots, N$,

$$\begin{pmatrix} \boldsymbol{F}_i \\ \boldsymbol{T}_i \end{pmatrix} = \sum_{j=1}^{N} \boldsymbol{\zeta}_{ij} \cdot \begin{pmatrix} \boldsymbol{U}_j \\ \boldsymbol{\Omega}_j \end{pmatrix}. \tag{A.1}$$

In a conglomerate, the particles touch each other, and some of the $\boldsymbol{\zeta}_{ij}$ components become infinite. Instead of using equation (A.1), it is therefore necessary to eliminate the forbidden degrees of freedom (relative motions). This is done by constructing the conglomerate friction as the sum of the relevant combinations of $\boldsymbol{\zeta}_{ij}$ only,

$$\boldsymbol{\zeta} = \sum_{i=1}^{N} \sum_{j=1}^{N} \mathbf{P}_i^{\mathrm{T}} \cdot \boldsymbol{\zeta}_{ij} \cdot \mathbf{P}_j. \tag{A.2}$$

The 6×6 friction matrix $\boldsymbol{\zeta}$ is finite at the contact, because the combinations of $\boldsymbol{\zeta}_{ij}$ in equation (A.2) correspond to motions that are free from the lubrication singularities. By inverting $\boldsymbol{\zeta}$, we obtain the conglomerate mobility,

$$\boldsymbol{\mu} = \boldsymbol{\zeta}^{-1}. \tag{A.3}$$

In the following, we construct the operators $\mathbf{P}_i$ for two different types of conglomerates. First, a rigid system is considered, for which all relative motions are excluded. Then, a conglomerate with spinning particles is analyzed.

A.1. Hydrodynamics of a rigid system

A rigid motion of a conglomerate made of N spheres is characterized by the translational velocity $\boldsymbol{U}$ of an arbitrarily chosen center of reference $\mathbf{R}$ and conglomerate rotational velocity $\boldsymbol{\Omega}$. Then, the translational and rotational velocities of the individual sphere centers, $i = 1, \ldots, N$, are given as

$$\boldsymbol{U}_i = \boldsymbol{U} + \boldsymbol{\Omega} \times (\mathbf{r}_i - \mathbf{R}), \tag{A.4}$$

$$\boldsymbol{\Omega}_i = \boldsymbol{\Omega}, \tag{A.5}$$

or equivalently,

$$\begin{pmatrix} \boldsymbol{U}_i \\ \boldsymbol{\Omega}_i \end{pmatrix} = \mathbf{P}_i \cdot \begin{pmatrix} \boldsymbol{U} \\ \boldsymbol{\Omega} \end{pmatrix}, \qquad i = 1, \ldots, N, \tag{A.6}$$

where the 6×6 matrices $\mathbf{P}_i$ are given by the relation,

$$\mathbf{P}_i = \begin{pmatrix} \mathbf{I} & \mathbf{P}_i^{tr} \\ 0 & \mathbf{I} \end{pmatrix}, \tag{A.7}$$

$$(\mathbf{P}_i^{tr})_{\alpha\beta} = \varepsilon_{\alpha\beta\gamma}(r_{i\gamma} - R_\gamma). \tag{A.8}$$

The total force $\boldsymbol{F}$ and torque $\boldsymbol{T}$ with respect to the center $\mathbf{R}$, exerted externally on the conglomerate, have the form,

$$\boldsymbol{F} = \sum_{i=1}^{N} \boldsymbol{F}_i, \tag{A.9}$$

$$T = \sum_{i=1}^{N} [T_i + (\mathbf{r}_i - \mathbf{R}) \times F_i] \qquad (A.10)$$

or equivalently,

$$\begin{pmatrix} F \\ T \end{pmatrix} = \sum_{i=1}^{N} \mathbf{P}_i^{\mathrm{T}} \cdot \begin{pmatrix} F_i \\ T_i \end{pmatrix}, \qquad (A.11)$$

where $^{\mathrm{T}}$ stands for the matrix transposition. By inserting equations (A.1) and (A.6) into equation (A.11), we relate the total external force and torque on the conglomerate to its translational and rotational velocities,

$$\begin{pmatrix} F \\ T \end{pmatrix} = \zeta \cdot \begin{pmatrix} U \\ \Omega \end{pmatrix}, \qquad (A.12)$$

with the conglomerate friction ζ given by equation (A.2). Writing the conglomerate velocities explicitly in terms of the corresponding components of the mobility $\mu = \zeta^{-1}$,

$$\begin{pmatrix} U \\ \Omega \end{pmatrix} = \begin{pmatrix} \mu^{tt} & \mu^{tr} \\ \mu^{rt} & \mu^{rr} \end{pmatrix} \cdot \begin{pmatrix} F \\ T \end{pmatrix}, \qquad (A.13)$$

and choosing the center of mass as the reference center, to obtain $T = \mathbf{0}$, we recover the relations (4) and (5), with the rigid-chain mobility matrices μ^{tt} and μ^{rt}.

A.2. Hydrodynamics of a chain made of beads

Let us now consider a chain of three beads. The sphere 2 touches the other spheres, but the spheres 1 and 3 are separated from each other and therefore are able to spin along $\hat{r}_{12}$ and $\hat{r}_{32}$, respectively. The motion of the chain is characterized by the translational velocity U of an arbitrary center of reference $\mathbf{R}$, the chain rotational velocity Ω, and also by the two spinning velocities ω_1 and ω_3. Then, the translational and rotational velocities of individual sphere centers are given by the relation,

$$U_i = U + \Omega \times (\mathbf{r}_i - \mathbf{R}), \qquad i = 1, 2, 3, \qquad (A.14)$$

$$\Omega_i = \Omega + \omega_i \hat{r}_{i2}, \qquad i = 1, 3, \qquad (A.15)$$

$$\Omega_2 = \Omega \qquad (A.16)$$

or equivalently,

$$\begin{pmatrix} U_i \\ \Omega_i \end{pmatrix} = \mathbf{P}_i \cdot \begin{pmatrix} U \\ \Omega \\ \omega_1 \\ \omega_3 \end{pmatrix}, \qquad i = 1, 2, 3, \qquad (A.17)$$

with the 6×8 matrices $\mathbf{P}_i$ defined with the use of the same equation (A.8) for $\mathbf{P}_i^{tr}$, but now differently than in equation (A.6),

$$\mathbf{P}_1 = \begin{pmatrix} \mathbf{I} & \mathbf{P}_1^{tr} & 0 & 0 \\ 0 & \mathbf{I} & \hat{r}_{12} & 0 \end{pmatrix}, \qquad (A.18)$$

$$\mathbf{P}_2 = \begin{pmatrix} \mathbf{I} & \mathbf{P}_2^{tr} & 0 & 0 \\ 0 & \mathbf{I} & 0 & 0 \end{pmatrix}, \qquad (A.19)$$

$$\mathbf{P}_3 = \begin{pmatrix} \mathbf{I} & \mathbf{P}_3^{tr} & 0 & 0 \\ 0 & \mathbf{I} & 0 & \hat{r}_{13} \end{pmatrix}. \qquad (A.20)$$

Then, equation (A.2) is used to evaluate the 8×8 chain friction matrix ζ. It relates the chain velocities U, Ω, ω_1 and ω_2, to the total external forces and torques (A.9) and (A.10), and the torque components $t_1 = T_1 \cdot \hat{r}_{12}$ and $t_3 = T_3 \cdot \hat{r}_{32}$,

$$\begin{pmatrix} F \\ T \\ t_1 \\ t_3 \end{pmatrix} = \zeta \cdot \begin{pmatrix} U \\ \Omega \\ \omega_1 \\ \omega_3 \end{pmatrix}. \qquad (A.21)$$

Evaluating the chain mobility $\mu = \zeta^{-1}$, we obtain,

$$\begin{pmatrix} U \\ \Omega \\ \omega_1 \\ \omega_3 \end{pmatrix} = \mu \cdot \begin{pmatrix} F \\ T \\ t_1 \\ t_3 \end{pmatrix}. \qquad (A.22)$$

In our system, the spheres are identical, $\mathbf{R}$ is the center-of-mass position, $T = \mathbf{0}$ and $t_1 = t_3 = 0$. Therefore, $\omega_1 = -\omega_3 = \omega$ and we obtain the relations (4)–(6).

References

[1] Kasper G, Niida T and Yang M 1985 *J. Aerosol Sci.* **16** 535
[2] Lasso I A and Weidman P D 1986 *Phys. Fluids* **29** 3921
[3] Geller A S, Mondy L A, Rader D J and Ingber M S 1993 *J. Aerosol Sci.* **24** 597
[4] Mondy L A, Geller A S, Rader D J and Ingber M 1996 *J. Aerosol Sci.* **27** 537
[5] Cichocki B and Hinsen K 1995 *Phys. Fluids* **7** 285
[6] Berg H C 2000 *Phys. Today* **53** 24
[7] Cisneros L, Dombrowski C, Goldstein R E and Kessler J O 2006 *Phys. Rev.* E **73** 030901(R)
[8] Taylor G I 1951 *Proc. R. Soc.* A **209** 447
[9] Purcell E M 1977 *Am. J. Phys.* **45** 3
[10] Childress S 1981 *Mechanics of Swimming and Flying* (Cambridge: Cambridge University Press)
[11] Pedley T J and Kessler J O 1992 *Annu. Rev. Fluid Mech.* **24** 313
[12] Becker L E, Koehler S A and Stone H A 2003 *J. Fluid Mech.* **490** 15
[13] Dreyfus R, Baudry J, Roper M L, Fermigier M, Stone H A and Bibette J 2005 *Nature* **437** 862
[14] Najafi A and Golestanian R 2004 *Phys. Rev.* E **69** 062901
[15] Gauger E and Stark H 2006 *Phys. Rev.* E **74** 021907
[16] Felderhof B U 2006 *Phys. Fluids* **18** 063101
[17] Tam D and Hosoi A 2007 *Phys. Rev. Lett.* **98** 068105
[18] Kim S and Karrila S J 1991 *Microhydrodynamics* (Boston: Butterworth-Heinemann)
[19] Kessler J O 1985 *Nature* **313** 218
[20] Kessler J O 1992 *Adv. Space Res.* **12** 33
[21] Felderhof B U 1988 *Physica* A **151** 1
[22] Cichocki B, Felderhof B U, Hinsen K, Wajnryb E and Bławzdziewicz J 1994 *J. Chem. Phys.* **100** 3780
[23] Cichocki B, Ekiel-Jeżewska M L and Wajnryb E 1999 *J. Chem. Phys.* **111** 3265
[24] Ekiel-Jeżewska M L and Wajnryb E 2006 *Arch. Mech.* **58** 489
[25] Ekiel-Jeżewska M L and Wajnryb E 2006 *Phys. Rev.* E **73** 046309
[26] Hocking L M 1964 *J. Fluid Mech.* **20** 129
[27] Cichocki B, Ekiel-Jeżewska M L, Nägele G and Wajnryb E 2004 *J. Chem. Phys.* **121** 2305
[28] Happel J and Brenner H 1991 *Low Reynolds Number Hydrodynamics* (Leyden: Kluwer–Academic)
[29] Jeffrey D J and Onishi Y 1984 *J. Fluid Mech.* **139** 261
[30] Ekiel-Jeżewska M L and Wajnryb E 2006 *Q. J. Mech. Appl. Math.* **59** 563
[31] Caflisch R E, Lim C, Luke J H C and Sangani A S 1988 *Phys. Fluids* **31** 3175
[32] Press W H, Teukolsky S A, Vetterling W T and Flannery B P 1992 *Numerical Recipes* (Cambridge: Cambridge University Press)